Kinematics and Verification of a Deboning Device

Debao Zhou[+], Wayne Daley[*] and Gary McMurray[*]

[+]Department of Electrical and Computer Engineering, University of Minnesota, Duluth, MN 55812
[*]FPTD/ATAS/GTRI, Georgia Institute of Technology, Atlanta, GA 30332-0823

Abstract—**Poultry deboning process is one of the largest employers in the United States and mainly involves human workers due to the unstructured nature of the task. For the automation of this process, a cutting device with the adaptive capability has been developed. In this paper, we focused on the kinematics of this device and the accuracy of the actual cutting point location. We validated the kinematic formulation and proofed the confidence of the accurate cutting. The applied verification method can be generalized to be applicable to general kinematics verification.**

***Index Terms* — kinematics, verification, deboning, robotic device.**

I. Introduction and Background

Kinematics verification is a task to make sure the designed robotic device can reach the position obtained using the kinematics with satisfied accuracy by assuming the steady-state error of the control system is zero. It is important because it can used to verify the correctness of the kinematics and the end-effector position accuracy of a complex mechanism. In this paper, the verification of kinematics of a deboning device is described.

The deboning procedure to harvest chicken breast meat (also called butterfly) is shown in Figure 1. Figure 1(a) shows a chicken with a marked front half. Figure 1(b) shows the processing line to manually harvest butterflies from front halves in a poultry plant. One of the harvested butterflies is shown in Figure 1(d). In this procedure, a front half is first cut away from a chicken and then put on a cone for the breast meat harvesting. After the shoulder joint connections are severed, the wing and breast meat are pulled away from the carcass as shown in Figure 1(c). Considering this process has to be manually repeated on approximately 300,000 of chickens each day, it is obviously very onerous. Moreover, due to the naturally deformable bodies, size difference and possible hard bone chips in meat, its automation is very challenging. One commercial solution has been provided by the Stork Gamco Inc. [1]. However, their method still belongs to the fixed automation category since they require the cutting motions be preset manually and thus, they cannot automatically adapt to individual bird size. Meyn Inc. [2] developed another cutting device with only one fixed motion for all the front halves deboning. In order to adapt to variations in the chicken size, Daley *et al*. [3] proposed a reference-point method to estimate the locations of the cutting trajectory. In this method, the reference points were obtained through the analysis of the computer images. Using a similar method, Heck [4] proposed to use a water-jet cutting method to cut chicken breast meat to obtain certain shapes according to the identified trajectory from computer images. Beyond chicken deboning, some researches have been carried out on the pork or beef such as [5] and [6]. Their pork and beef deboning methods are to cut through everything including hard bones. So they are not deboning process.

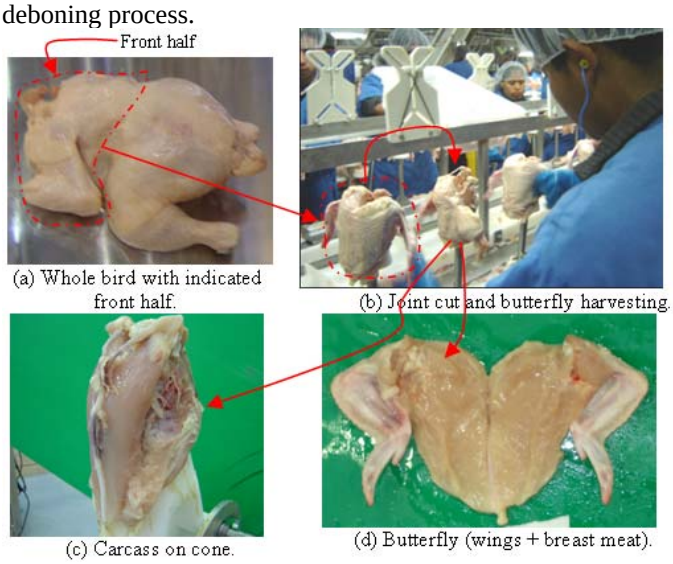

Figure 1: Illustration of the harvesting of chicken butterfly.

In this research, through the understanding of the anatomy of chicken shoulder joints, a new processing method associated with a simple mechanism has been developed [7]. Considering the procedure to harvest the breast meat, five working stations are applied as shown in Figure 2. The first one is the vision station which is used to identify the joints' locations. The second is the scapula cut station. The next two are for the left and right clavicle cuts. The last one is for the joint cut. The detailed joint cutting prototype is shown in Figure 3.

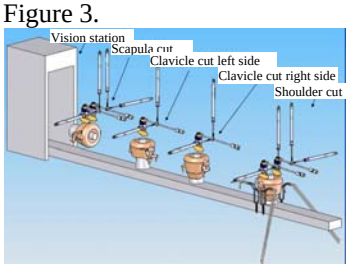

Figure 2: Front half deboning system diagram.

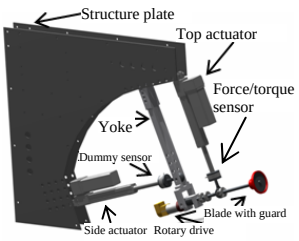

Figure 3: Joint cutting device.

The cutting device has been designed as shown in Figure 4 and the electrical wiring system is shown in Figure 5. The control of the translation system is realized using NI PCI-6236 M series card on a Linux system [8]. The hardware connection

illustration is shown in Figure 6. The control software is the Scilab with RTAI real-time control system [9].

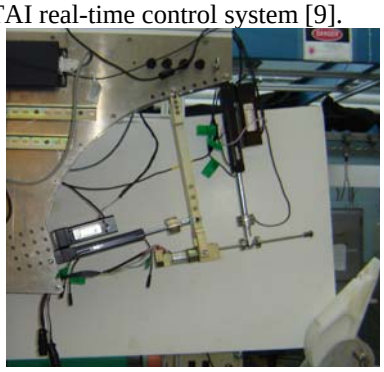

Figure 4: Cutting device.

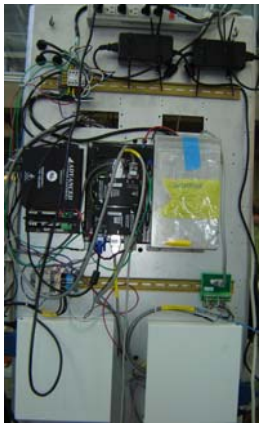

Figure 5: Electrical wiring system.

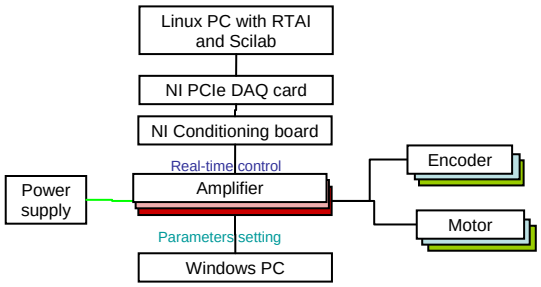

Figure 6: Illustration of the electrical wiring system.

In the reminder of this paper, the formulation of the system kinematics is shown in Section II first. The results obtained from the kinematics realization are presented in Section III. The verification of the kinematics using an ABB robot is described in Section IV. After the discussion and analysis, conclusions are drawn in Section V.

II. Kinematics Formulation

The kinematic skeleton sketch of the joint-cutting device is shown in Figure 7. The cutting tool is a 2-link mechanism, links *OP* and *PC*. The linkage is driven by two translational actuators. Frame *OXZ* is fixed in the space, where *Y* is not shown due to the plannar mechanism. Point *O* is a universal joint connected to a space-fixed location and point *P* is another universal joint. The device has 3 DOFs, rotations around points *O*, *P* and the rotation around axis *PC*, where point *C* is called center of the cutting edge in this paper. The driven system includes two electrical actuators, called up-down actuator and left-right actuator, and one rotary motor. The up-down actuator, which connects to the handle at point P_2, is mainly for the cutting motion. The left-right actuator, which connects to the yoke at point P_1, is mainly for size adaptation motion. The other side of each linear actuator is fixed to the structure plate through one pin joint to make the two actuators and the yoke rotate freely relative to the points *O*, O_1 and O_2, respectively.

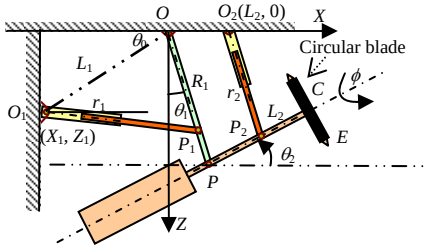

Figure 7: Schematic illustration of the cutting device.

In the following, subscript 1 is for the left-right actuator and subscript 2 expresses the parameters for the up-down actuator. In *OXZ* frame, the notations are: *O* (0, 0) is the origin of the space-fixed frame. O_1 (X_1, Z_1) is the base of the left-right actuator. O_2 (L_2, 0) is the base of the up-down actuator. P_1, P_2 are the locations of the linear actuators connecting to the yoke and handle, where $OP_1 = R_1$, $OP = R$, $PP_2 = L_2$, $PC = L$, $O_1P_1 = r_1$, $O_2P_2 = r_2$, $OO_1 = L_1$, $\angle ZOP = \theta_1$, and $\angle XPC = \theta_2$. *C* (*x*, *z*) is the center of the rotary blade and the radius of the circular blade is R_c. ϕ is used to express the rotation of the cutter which is not considered in this paper.

Three sets of generalized coordinates are identified: {$\Re$: $q_1 = r_1$, $q_2 = r_2$, $q_3 = \phi$ }, {Θ: $q_1 = \theta_1$, $q_2 = \theta_2$, $q_3 = \phi$ } or {Λ: $q_1 = x$, $q_2 = z$, $q_3 = \phi$}, where q_1, q_2, q_3 are generalized coordinate. The initial position of the system is the posture where *OP* is on *OZ*, and $O_2O//PP_2//O_1P_1$ ($OP//O_2P_2$). The forward kinematics is from $\Re$ to Λ and the inverse kinematics is from Λ to $\Re$.

A. Relationship between Λ and Θ

The relationship between *x*, *z* at point *C* and θ_1, θ_2 can be obtained as

$$\begin{bmatrix} x \\ z \end{bmatrix} = L\begin{bmatrix} c_2 \\ -s_2 \end{bmatrix} + R\begin{bmatrix} s_1 \\ c_1 \end{bmatrix}, \quad (1)$$

and at point *E*, the edge of the circular blade on plane *OXZ*,

$$\begin{bmatrix} x_e \\ z_e \end{bmatrix} = L_c\begin{bmatrix} c_{2-3} \\ -s_{2-3} \end{bmatrix} + R\begin{bmatrix} s_1 \\ c_1 \end{bmatrix} \quad (2)$$

where $L_c = \sqrt{L^2 + R_c^2}$ $s_1 \equiv \sin(\theta_1)$, $c_1 \equiv \cos(\theta_1)$, $s_2 \equiv \sin(\theta_2)$, $c_2 \equiv \cos(\theta_2)$, $s_{2\text{-}3} \equiv \sin(\theta_2\text{-}\theta_3)$, $c_{2\text{-}3} \equiv \cos(\theta_2\text{-}\theta_3)$ and $\theta_3 = \tan^{-1}(R_c/L)$. By solving θ_1 and θ_2, there are

$$\theta_1 = \sin^{-1}\left(\frac{x_e^2 + z_e^2 + R^2 - L_c^2}{2R\sqrt{x_e^2 + z_e^2}}\right) - \sin^{-1}\left(\frac{z_e}{\sqrt{x_e^2 + z_e^2}}\right), \quad (3)$$

$$\theta_2 = \sin^{-1}\left(\frac{x_e^2 + z_e^2 + L_c^2 - R^2}{2L_c^2\sqrt{x_e^2 + z_e^2}}\right) - \sin^{-1}\left(\frac{x_e}{\sqrt{x_e^2 + z_e^2}}\right) + \tan^{-1}(Rc_2 / L) \quad (4)$$

.

The relationship between the velocity of the cutting point of the rotary blade and the angular velocity of the mechanism is

$$\begin{bmatrix} \dot{x} \\ \dot{z} \end{bmatrix} = \begin{bmatrix} -Ls_2 & Rc_1 \\ -Lc_2 & -Rs_1 \end{bmatrix}\begin{bmatrix} \dot{\theta}_2 \\ \dot{\theta}_1 \end{bmatrix}, \quad (5)$$

or

$$\begin{bmatrix}\dot{\theta}_2\\ \dot{\theta}_1\end{bmatrix}=\begin{bmatrix}-Ls_2 & Rc_1\\ -Lc_2 & -Rs_1\end{bmatrix}^{-1}\begin{bmatrix}\dot{x}\\ \dot{z}\end{bmatrix}. \quad (6)$$

B. Relationship between $\mathfrak{R}$ and Λ

Using the law of Cosine on triangle OO_1P_1, there is

$$r_1^2 = L_1^2 + R_1^2 + 2L_1R_1\sin(\theta_1-\theta_0). \quad (7)$$

Thus

$$\dot{r}_1 = L_1R_1\cos(\theta_1-\theta_0)\dot{\theta}_1/r_1. \quad (8)$$

The vectors $\mathbf{r}_{OP_2}$ and $\mathbf{r}_2$ can be expressed as

$$\mathbf{r}_{OP_2} = \begin{bmatrix}Rs_1+L_2c_2 & 0 & Rc_1-L_2s_2\end{bmatrix}^T,$$

$$\mathbf{r}_2 = \begin{bmatrix}Rs_1+L_2c_2-L_2 & 0 & Rc_1-L_2s_2\end{bmatrix}^T,$$

thus

$$r_2^2 = \left(Rs_1+L_2c_2-L_2\right)^2+\left(Rc_1-L_2s_2\right)^2. \quad (9)$$

There is

$$r_2\dot{r}_2 = \left(Rs_1+L_2c_2-L_2\right)\left(Rc_1\dot{\theta}_1-L_2s_2\dot{\theta}_2\right)+\left(Rc_1-L_2s_2\right)\left(-Rs_1\dot{\theta}_1-L_2c_2\dot{\theta}_2\right).$$

So

$$\dot{r}_2 = \frac{1}{r_2}\begin{bmatrix}\left(Rs_1+L_2c_2-L_2\right)Rc_1-\left(Rc_1-L_2s_2\right)Rs_1\\ -\left(Rs_1+L_2c_2-L_2\right)L_2s_2-\left(Rc_1-L_2s_2\right)L_2c_2\end{bmatrix}^T\begin{bmatrix}\dot{\theta}_1\\ \dot{\theta}_2\end{bmatrix}, \quad (10)$$

and

$$\dot{\theta}_2 = \frac{r_2\dot{r}_2-\left(Rs_1+L_2c_2-L_2\right)Rc_1-\left(Rc_1-L_2s_2\right)Rs_1\dot{\theta}_1}{\left(Rs_1+L_2c_2-L_2\right)L_2s_2-\left(Rc_1-L_2s_2\right)L_2c_2}. \quad (11)$$

From the above relationships, both the direct kinematics and inverse kinematics can be formulated.

From (7), there is

$$\theta_1 = \sin^{-1}\left(\frac{r_1^2-L_1^2-R_1^2}{2L_1R_1}\right)+\theta_0. \quad (12)$$

From (9), there is

$$r_2^2 = R^2+2L_2^{\,2}-2RL_2s_1+2\left(Rs_1-L_2\right)L_2c_2-2RL_2c_1s_2. \quad (13)$$

Or

$$\frac{\left(L_2-Rs_1\right)}{\sqrt{\left(L_2-Rs_1\right)^2+\left(Rc_1\right)^2}}c_2+\frac{Rc_1}{\sqrt{\left(L_2-Rs_1\right)^2+\left(Rc_1\right)^2}}s_2 = \frac{R^2+2L_2^{\,2}-r_2^2-2RL_2s_1}{2L_2\sqrt{\left(L_2-Rs_1\right)^2+\left(Rc_1\right)^2}}. \quad (14)$$

Set

$$\theta_4 = \tan^{-1}\left[\frac{\left(L_2-Rs_1\right)}{Rc_1}\right]$$

There is

$$\sin(\theta_2+\theta_4) = \frac{R^2+2L_2^{\,2}-r_2^2-2RL_2s_1}{2L_2\sqrt{\left(L_2-Rs_1\right)^2+\left(Rc_1\right)^2}}. \quad (15)$$

i.e.

$$\theta_2 = \sin^{-1}\left[\frac{R^2+2L_2^{\,2}-r_2^2-2RL_2s_1}{2L_2\sqrt{\left(L_2-Rs_1\right)^2+\left(Rc_1\right)^2}}\right]-\theta_4. \quad (16)$$

Set the encoder counts of the two motors are E_1 and E_2 and the coefficient from encoder count to the translation distance of the linear actuator is κ, there are

$$r_1 = \kappa E_1 \text{ and } r_2 = \kappa E_2 \quad (17)$$

Then the direct kinematics in the sense of getting the coordinate of Points *C* and *E* using the encoder counts can be calculated from (17), (12), (16), (1) and (2) and the inverse kinematics in the sense of getting the encoder counts using the coordinate of Point *E* can be obtained from (3), (4), (7), (9) and (17).

III. Kinematics Realization

Based on the mechatronics system, the control program has been developed. Given the desired trajectory as the green trajectory in Figure 8, the actual trajectories were obtained as the red line in Figure 8 expressed using the actual encoder counts. The results show that the desired encoder counts have been realized. Further results showed that the steady-state error of the control system is zero. However, it is still not sure whether the actual cutting point, i.e. Point *C*, reaches the desired location. Thus further verification is required.

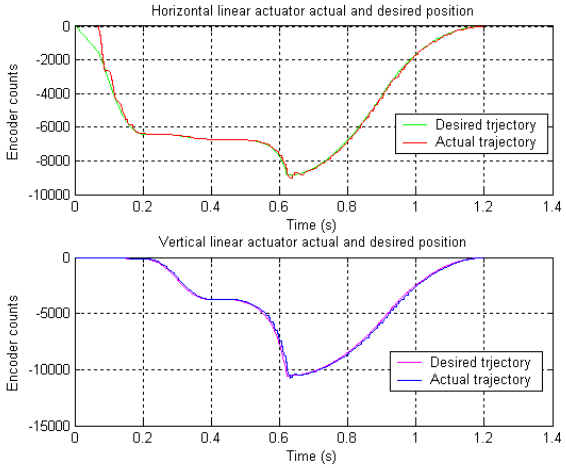

Figure 8: Desired and actual trajectory in senses of the encoder counts.

IV. Kinematics Verification

4.1 Robot Calibration and Frame Combination

In order to verify the accuracy of the actual cutting point locations, the initial posture of the actual cutting device is set to the one used in simulation. The following method is used to make sure the two initial postures (actual one and simulated one) are the same.

Figure 9 shows the initial posture of the actual deboning device where the shaded areas represent the reference frame. An inclinometer is used to measure the inclined angle of the frame and make the angle relative to the (absolute) horizontal line at 16.0°. The resolution of the inclinometer is 0.1°. Next through the adjustment of the horizontal cylinder position, the angle of the horizontal cylinder is fixed at 16.0° indicated by the horizontal homing sensor. The homing sensor is fixed on the sleeve of the linear actuator. This makes the yoke perpendicular to OO_2. By adjusting the length of the vertical cylinder, i.e. by adjusting the homing sensor location, the angle of the cutting link (handle *PC*) can be adjusted to 16.0° to make the handle (cutting link) perpendicular to the yoke. Since the length of PP_2 is equal to the length of OO_2,

rectangle OO_2P_2P is formed. This can be further verified by measuring the angle of O_2P_2 relative to gravity as 74.0°. This initial posture is used to verify the accuracy of the commanded positions by giving encoder counts.

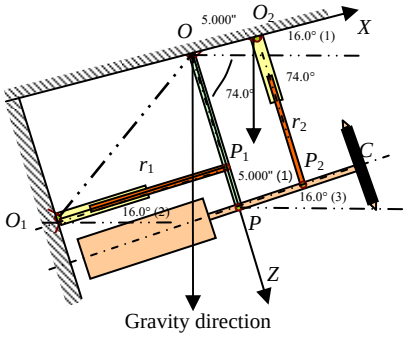

Figure 9: Initial position of the cutting device.

An ABB IR140 robot [10] was used to measure the cutting point coordinates and the following procedure was used to make sure the accuracy of the robot measurement. First, an accurate mechanical pointer was designed and installed on the robot for position measurement. Second, a 4–point method [10] was used to define the sharp point of the pointer as the tool's center point (TCP) [10].

It has been verified that the repeatability of the robot to approaching a point is within 0.05mm. This was done through the following method: In the initial position of the cutting device, the TCP was controlled to approach the cutting point as shown in Figure 10(a) and the position coordinate was recorded in the robot. By approaching the same point several times and comparing the repeatability of the obtained coordinates, the repeatability of the robot could be verified.

We also verified the repeatability of distance measurements. The tool we used was a standard gauge with known edge lengths. The robot was used to measure the corner points of gauge which was fixed in the working space of the cutting device as shown in Figure 10(b).

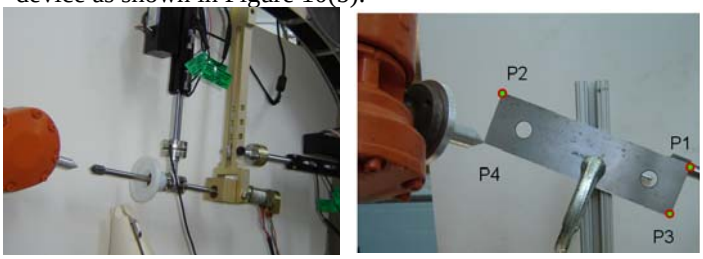

(a) (b)

Figure 10: Combining robot frame with device frame.

The motion plane of point *C* in Figure 9 is independent of the robot base frame. However, by re-defining the cutting device base frame (*OXYZ*) as the robot work-object frame in robot coordinate system, the TCP coordinate will be the same as the cutting point *C*. A three-point method was used to define the work-object frame of the robot to attach the robot work-object frame to the cutting device: (1) Put the TCP just at point *C* in the initial posture and record this point at X_1; (2) Control the end effector of the cutting device to move in the *OX* direction as shown in Figure 9 and measure Point *C* location using the TCP and mark the point as X_2; (3) Control the cutting device to make it move along the *OZ* axis as shown in Figure 9, and mark the point as Y_1 in the robot. Based on point X_1, X_2, and Y_1, the robot object frame was defined as the origin at point X_1, X_1Y_1 as the *y* axis, X_1X_2 as the *x* axis of the robot work object frame and the *z* axis of the work object frame was obtained using the right-hand rule.

In order to verify the accuracy of the obtained work-object frame, the 4th corner (P_4 in Figure 10(b)) of the rectangular gauge was measured based on the work-object frame defined by the other three corner points. Note that geometry of the rectangular gauge provides the exact location of the P_4 relative to P_1, P_2 and P_3.

4.2 Coordinate Measurement

Using the defined work-object frame, which was the same as the base frame of the cutting device, several points in the work space of the deboning device as shown in Figure 11 were measured to verify the kinematics. In Figure 11, point 6 is the left-lower limit of the work space, 7 the left-upper limit, 8 the right-upper limit, 9 the right-lower limit, 10 working space center point and 1, 2, 3 are the points to define the work object frame.

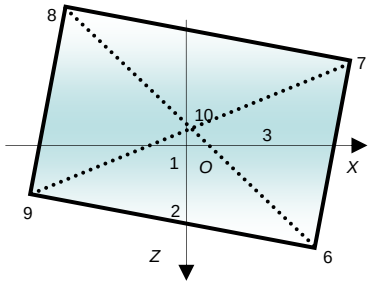

Figure 11: Measurement points in the cutting workspace for kinematic verification.

From Section 4.1, we know that the physical coordinate obtained by the robot in the robot work-object frame is the same in value as the coordinate expressed in the cutting device base frame. Moreover, using the encoder feedback of the device relative to the homing position, the cutting point's coordinate can be computed using the direct kinematics formulation. If the kinematics of the system is correct and the steady-state error of the position control of the cutting device is zero, the coordinates of the points obtained from the robot measurement and the kinematic computation should be the same.

The procedure to verify the direct kinematics is as follows: (i) Estimate the encoder counts of the two motors for the interested points in Figure 11; (ii) Using (17), (16), (12) and (1) to calculate the desired coordinate (x_d, x_d, z_d); (iii) Input the desired encoder counts to the Linux machine control program and use Scilab/RTAI [9] to generate the executable control program; (iv) Run homing program at less twice to make sure the cutting device in the homing position; (v) Run the control program to realize the desired encoder counts; (vi) Using ABB robot to measure the desired position and record as (x_{ai}, z_{ai}). Once we have the data (x_{di}, z_{di}) and (x_{ai}, z_{ai}), where *i* is the measure sequence number, we can process the data and make the analysis.

4.3 Data Processing – Robot Calibration

The actual gauge distance and the measured distance as shown in Figure 10 (b) are listed in Table 1 and the distance error processing results are shown in Table 2. Note the unit is mm.

Table 1, Actual gauge distance and measured distance.

	P_1 to P_2	P_1 to P_3	P_2 to P_3
Actual distance	152.400	41.275	157.890
Measured #1	151.408	40.790	157.043
Measured #2	151.708	40.918	157.078
Measured #3	151.475	40.995	157.472
Measured #4	151.528	41.214	157.318
Measured #5	151.682	40.789	157.261

Table 2, Process of the distance-error data.

	P_1 to P_2	P_1 to P_3	P_2 to P_3
Mean	-0.840	-0.334	-0.656
Standard error	0.059	0.079	0.079
Median	-0.872	-0.357	-0.629
Standard deviation	0.131	0.176	0.177
Sample variance	0.017	0.031	0.031
Kurtosis	-2.457	0.617	-1.405
Range	0.301	0.425	0.428
Minimum	-0.992	-0.486	-0.847
Maximum	-0.692	-0.061	-0.419
Sum	-4.199	-1.669	-3.281
Count	5.000	5.000	5.000
Confidence level(99.0%)	0.270	0.363	0.364

For the distance from P_1 to P_2, the difference between the measured one and the actual one (152.400mm) is about 1.120mm with 99% confidence; For the distance from P_2 to P_3, the difference between the measured one and the actual one (41.275mm) is about 0.797mm with 99% confidence; For the distance from P_1 to P_3, the difference between the measured one and the actual one (157.890mm) is about 1.120mm with 99% confidence.

When building the frame on $P_1P_2P_3$, the actual coordinate of point P_4 is (152.400mm, 41.275mm, 0). The measured coordinates is within 1.357mm error with 99% confidence. These results proofed the accuracy of the robot measurement and the accuracy of the built robot frame on the deboning device.

4.4 Data Processing - Coordinate Measurement

To determine the magnitude of the position error of the cutting blade center point (Point *C* in Figure 7), we performed a 2^2 factorial design [11]. The measurements were randomized with five replicates for each position for a total of twenty five observations. The levels for the 2^2 factorial design correspond to the points 6, 7, 8 and 9 in Figure 11. The center point corresponds to the point 10 on the same figure. The levels cover the entire cutting span of the device. The response variable is the error of the cutting blade axis measured as the Euclidean distance between the actual and homing position. The factors are the *X* and *Z* coordinates of the cutting blade center point, assuming that the *Y* coordinate is constant. The data are shown in Table 3.

Using Minitab® R15, we performed an ANOVA on the data. The null hypothesis is that the error is constant and independent of the position of the cutting blade axis. The unit of the data in Table 3 is millimeter. The *p* value determines the appropriateness of rejecting the null hypothesis in a hypothesis test. It ranges from 0 to 1. The smaller the p-value is, the smaller the probability that rejecting the null hypothesis is a mistake.

Table 3, Measured coordinates.

Point #	6	7	8	9	10
x_a	24.987	22.617	-36.368	-33.941	-2.927
x_{d1}	25.030	22.170	-36.680	-34.050	-3.160
x_{d2}	24.850	22.330	-36.890	-34.090	-3.140
x_{d3}	24.800	22.320	-36.520	-34.170	-3.060
x_{d4}	24.770	22.020	-36.760	-33.180	-3.250
x_{d5}	24.820	22.150	-36.800	-33.710	-3.420
z_a	25.354	-45.517	-46.908	25.797	-9.005
z_{d1}	25.850	-44.600	-46.690	26.320	-8.060
z_{d2}	25.700	-44.360	-46.660	26.240	-8.270
z_{d3}	25.990	-44.400	-46.420	26.280	-8.200
z_{d4}	26.010	-44.430	-46.830	26.390	-8.140
z_{d5}	25.980	-44.280	-46.850	26.250	-8.400
y_a	0.000	0.000	0.000	0.000	0.000
y_{d1}	0.230	-0.120	2.030	1.430	0.740
y_{d2}	-0.220	-0.230	1.940	1.780	0.730
y_{d3}	-0.280	-0.050	1.950	1.360	0.720
y_{d4}	-0.320	-0.200	2.280	1.490	0.680
y_{d5}	-0.170	-0.260	2.240	1.400	0.730

The summary of the ANOVA test were obtained using *alpha-level* < *0.01* for significance testing. The descriptive statistics of the data with unit mm is as the follows:

Variable	Mean	Minimum	Maximum	Range
x	-5.13	-36.37	24.99	61.36
z	-10.06	-46.91	25.8	72.71
Error	1.34	0.432	2.315	1.882

The errors with the observation order are plotted in Figure 12. It is a graphical expression of the error data in Table 3.

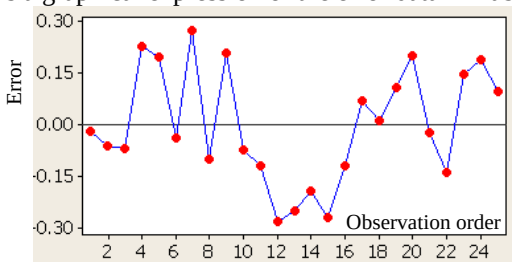

Figure 12: Position error plotted with observation order.

The relationship between the error and the error percentage are shown in Figure 13. A linear relationship is obtained. This proofs that the data is in normal distribution.

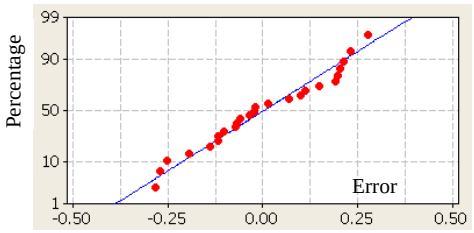

Figure 13: Relationship between residual and percentage.

Table 4, Error statistic results about the predictors *x* and *z*.

Predictor	Coef	SE Coef	*t*	*p*
Constant	1.184	0.0341	34.75	0.000
x	-0.0165	0.00122	-13.55	0.000
z	-0.00712	0.000999	-7.13	0.000

Using the measurement errors of the *x* and *z* coordinates as predictors, the results are shown in Table 4. From the "Coef" column, the regression equation is

$$Error = 1.18 - 0.0165\,x - 0.00712\,z$$

with standard deviation at 0.160285 and regression linearity 91.7%. The "SE Coef" stands for "standard error of coefficient" or "standard deviation of the estimate of a regression coefficient". It measures how precisely the data can estimate the coefficient's unknown value. The *t* value is obtained through the dividing of the coefficient by its standard error. It is observed that the *p*-value associated with this *t*-statistic is less than the *alpha-level*. That concludes that the coefficient is significantly different from zero or the results show that the null hypothesis is rejected, which means that the error changes with the position of the cutting blade axis, reaching its maximum value at the lowest level of both coordinates. The interaction is negligible.

V. Conclusions

In order to achieve an accurate end-effector position, the errors between the actual and the desired ones, can normally be minimized or eliminated by the controller. However, this still cannot ensure the exact position in the case that the desired one is calculated using the kinematics formulation based on the encoder feedback due to the reasons such as the mistakes in the kinematics formulation, offset of the initial position, backlash in the mechanism, etc. The end-effector position has to be measured and verified using an external device.

In this paper, we formulated the kinematics of a deboning device, proofed the correctness of the kinematics and verified its accuracy. Moreover, an ABB R140 robot had been used to verify the position accuracy. Using the robot with verified acceptable accuracy, a 2^2 factorial design method was applied. The obtained data was in the normal distribution. The statistic results show that the error is within 1.88mm and the error changes with the position of the cutting blade axis.

Since we got the error distribution and evaluated the influence factors, we can provide certain adjustment. This research also provides a basic method for kinematics verification.

Acknowledgement

This project was supported by the State of Georgia through the Agriculture Technology Research Program at the Georgia Tech Research Institute.

References

[1] Stork Gamco, Inc, http://stork.com/gamco/page.html?id =7610, March 2009.

[2] Meyn Food Processing Technology, *http://www. meyn.nl/index.php?option=com_content&task=view&id=123&Itemid=34*, Jan. 2007.

[3] W. Daley, T. He, K-M Lee and M. Sandlin, "Modeling of the natural product deboning process using biological and human models," in the *Proceedings of 1999 IEEE/ASME International Conference on Advanced Intelligent Mechatronics*, 19-23 Sept. , 1999, pp. 49 – 54.

[4] B. Heck, "Automated chicken processing: machine vision and water-jet cutting for optimized performance," *IEEE Control Systems Magazine*, 26(3), June, 2006, pp. 17-19.

[5] P. G. Dempsey and R. W. McGorry, "Investigation of a pork shoulder deboning operation," *Journal of Occupational and Environmental Hygiene*, vol 1, 2004, pp. 167-172.

[6] R. W. McGorry, P. C. Dowd and P. G. Dempsey, "The effect of blade finish and blade edge angle on forces used in meat cutting operations," *Applied Ergonomics*, Elsevier publications, vol. 35, 2005, pp. 71-77.

[7] D. Zhou, J. Holmes, W. Holcombe, K-M Lee and G. McMurray, "Automation of Bird Front Half Deboning Procedure: Design and Analysis," in *the Proceedings of the 12th IFToMM World Congress*, Besançon (France), 18-21, June 2007.

[8] National Instruments, "*NI 6236 User Manual*", Part Number,371948A-01, May 2006.

[9] R. Bucher, S. Mannori and T. Netter,"*RTAI-Lab tutorial: Scilab, Comedi, and real-time control*", https://www.rtai.org/RTAILAB/RTAI-Lab-tutorial.pdf, accessed March 2009.

[10] Product Manual IRB 140, ABB Robotics Products AB publication, article number: 3HAC 7564-1 issue: M2000, 2000.

[11] http://en.wikipedia.org/wiki/Factorial_experiment, accessed March 2009.